Progress In Electromagnetics Research Letters, Vol. 111, 61–70, 2023

A Novel Dual-Band Series-Fed Antenna Array with Independently Controllable Beam Direction

Chen-Xi Wang and Dong Chen*

Abstract—In this paper, a novel dual-band series-fed array (SFA) has been proposed. By introducing a new dual-band series-fed network (SFN) consisting of uniform transmission lines (TLs) and C-sections, independent beam direction can be realized. The design procedure for the proposed dual-band SFA has also been presented in this paper. To validate the design method, a prototype antenna has been fabricated and measured. The experimental results verify the performance of the proposed dual-band SFA.

1. INTRODUCTION

For the purpose to improve the performance of wireless systems, antenna arrays have been widely used in modern wireless equipment. Meanwhile, the rapid development of advanced wireless communication standards requires antenna arrays with dual-band or multi-band operation [1].

In general, there are two types of feeding structure: parallel-fed type [2–5] and series-fed type [6–17]. For the parallel-fed arrays (PFAs), if the number of antenna elements is N, and the phase difference between antenna elements is φ, the required maximum phase shift is $(N - -1) \times \varphi$. Compared with PFAs with the same number of antenna elements, series-fed arrays (SFAs) employ shorter feed lines with smaller circuit size and lower attenuation loss. For SFAs, the phase shift is the same as the phase φ for each antenna element, and it is easier to realize large beam angle.

For dual-band application, SFAs can be constructed by two series-fed networks (SFNs) with two input ports [6], two SFNs with one input port [7, 8], or single SFN [9–16]. In [6], by etching longitudinal slots on two different layers of substrate integrated waveguide (SIW), a dual-band SFA is devised. However, two SIW power dividers are demanded for these two slotted arrays. To avoid two input ports, frequency selective networks have been embedded to separate two operating frequencies [7, 8]. In [6–8], these methods all require two different antenna arrays and two different SFNs for dual-bands with a multi-layer structure, which results in large circuit area and high fabrication cost. Thus, SFAs with single SFN have been developed. As well known, travelling-wave antenna is a promising choice to realize a steerable radiation pattern within wide frequency band, such as leaky-wave antennas [9–13]. However, this type of antennas can hardly control the beam angles of different frequencies freely, and large length is usually needed by the travelling-wave antenna to keep sufficient radiation efficiency.

As another option, the standing-wave dual-band SFAs with single SFN are getting more and more research attentions [14–16]. In [14], a dual-frequency series-fed patch antenna array based on a periodic structure is proposed. However, this type can only achieve very close frequencies. In [15], a single-port dual-band SFA operating at multiples of the fundamental frequency is proposed. It consists of a lower band SFA and two higher band SFAs coupled to the feeding circuit. In [16], a novel dual-band SFA is devised by selecting proper coupling regions between the feeding line and radiating patches.

Received 11 April 2023, Accepted 12 June 2023, Scheduled 27 June 2023

* Corresponding author: Dong Chen (chendong@njupt.edu.cn).

The authors are with the College of Electronic and Optical Engineering, Nanjing University of Posts and Telecommunications, Nanjing, China.

In this paper, an SFA using a new dual-band series-fed network (SFN) composed of uniform transmission lines (TLs) and C-sections is presented. The proposed antenna exhibits good performance verified by the measured results, including independent beam direction and simple structure for easy fabrication.

2. DESIGN PRINCIPLE AND ANALYSIS FOR DUAL_BAND SFA

2.1. Proposed SFN on C-Section Lines

A new dual-band SFN on C-section lines is proposed in this section. In this work, two SFN unit structures are taken into consideration in the design, which consist of two and three C-sections in Figures 1(a) and (b), respectively. The C-sections with the even-/odd-mode impedance Z_{0e}/Z_{0o} and electrical length θ_c have all-pass characteristic and simple configuration. The uniform TLs with characteristic impedance Z_0 and electrical length θ_1 and θ_2 are used to connect the antenna element and separate the C-sections.

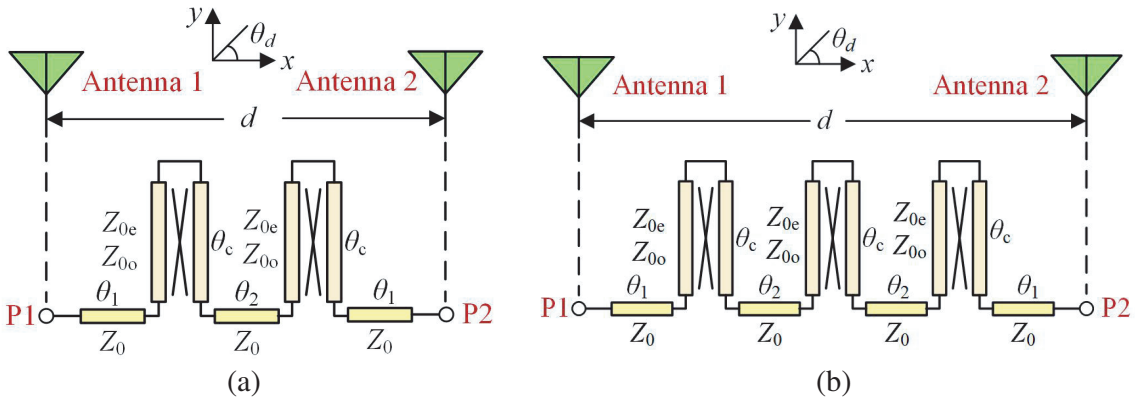

Figure 1. Schematic of proposed SFN unit for dual-band SFA using C-Section lines. (a) Structure 1: two C-Sections. (b) Structure 2: three C-Sections.

Based on the phase properties of uniform TLs and C-sections [17, 18], the design formulas for the proposed dual-band SFA on the SFN in Figure 1(a) are derived as

$$\begin{cases} 2m\pi + k_0 d\cos\theta_{d1} = 4\tan^{-1}\left(\dfrac{\tan(\theta_c)}{\sqrt{\rho}}\right) + \theta_{TL} \\ 2n\pi + k_0 d\cos\theta_{d2} = 4\tan^{-1}\left(\dfrac{\tan(\theta_c/n_f)}{\sqrt{\rho}}\right) + \dfrac{\theta_{TL}}{n_f} \end{cases} \tag{1}$$

where k_1 is the free-space wave number with respect to operating frequency f_1; d is the distance between antenna elements; θ_{d1} and θ_{d2} are the beam directions at the two operating frequencies f_1 and f_2 ($f_1 < f_2$); $\theta_{TL} = 2\theta_1 + 2\theta_2$, $n_f = f_1/f_2$; and ρ is the impedance ratio. The relationship between Z_{0e}/Z_{0o} and ρ is

$$Z_{0e} = Z_0\sqrt{\rho} \quad \text{and} \quad Z_{0o} = Z_0/\sqrt{\rho} \tag{2}$$

The design formulas for the proposed dual-band SFA based on structure 2 in Figure 1(b) can also be derived as:

$$\begin{cases} 2m\pi + k_0 d\cos\theta_{d1} = 6\tan^{-1}\left(\dfrac{\tan(\theta_c)}{\sqrt{\rho}}\right) + \theta_{TL} \\ 2n\pi + k_0 d\cos\theta_{d2} = 6\tan^{-1}\left(\dfrac{\tan(\theta_c/n_f)}{\sqrt{\rho}}\right) + \dfrac{\theta_{TL}}{n_f} \end{cases} \tag{3}$$

In Formulas (1) and (3), it can be found that there are three unknown variables (ρ, θ_{TL}, and θ_c). By taking the parameter θ_{TL} to be free variable, the design curves of the proposed SFN unit for specified

$\theta_{d1} = 90°$, $\theta_{d2} = 90°$, $n_f = f_1/f_2 = 0.6$ ($f_1 = 2.1\,\text{GHz}$ and $f_2 = 3.5\,\text{GHz}$), $d = 0.35\lambda_0$ ($m = 1$ and $n = 2$) based on (1) and (3) are shown in Figure 2. $d = 0.35\lambda_0$ takes both the gain in the lower band and grating lobe in the higher band into account.

In Figure 2(a), ρ decreases first and then increases with the increase of θ_{TL} for structure 1. Thus, ρ achieve its minimum at $\theta_{TL} = 135°$. Compared with structure 1, structure 2 can achieve smaller ρ and θ_{TL} when $\theta_{TL} < 135°$. The smaller ρ means weaker coupling which is easier to be implemented, and the smaller θ_{TL} means the shorter longitudinal length of the proposed SFN unit. Figure 2(b) shows θ_c versus θ_{TL}. It can be found that structure 2 can always achieve smaller θ_c than structure 1 under the same θ_{TL}. The smaller θ_c means the shorter transversal length. To verify the proposed design method, Figure 2(c) shows the simulated phase responses of three solutions as denoted in Figures 2(a) and (b). They all precisely achieve $\varphi_1 = 360°$ and $\varphi_2 = 720°$ at the $f_1 = 3.5\,\text{GHz}$ and $f_2 = 3.5\,\text{GHz}$, respectively. Then, the specified broadside radiations at f_1 and f_2 can be flexibly obtained as required.

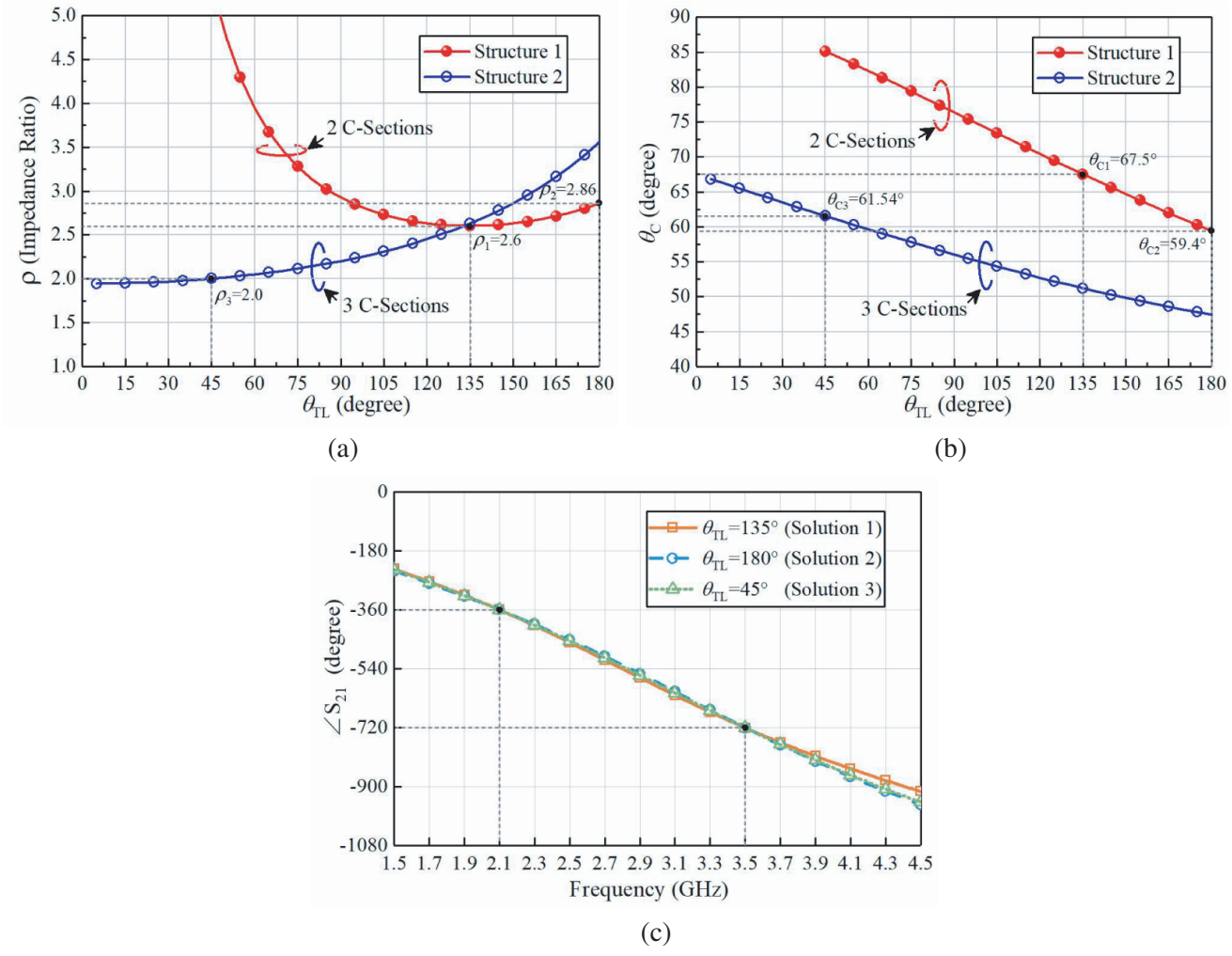

Figure 2. Design curves of the proposed SFN unit for specified $\theta_{d1} = 90°$, $\theta_{d2} = 90°$, $n_f = f_1/f_2 = 0.6$ ($f_1 = 2.1\,\text{GHz}$ and $f_2 = 3.5\,\text{GHz}$), $d = 0.3\lambda_0$ ($m = 1$ and $n = 2$). (a) ρ versus θ_{TL}. (b) θ_c versus θ_{TL}. (c) Simulated results.

2.2. Design of Dual-Band SFA

In this section, the design and analysis of a proposed dual-band SFA with four elements are presented. The operating frequencies are set to 2.1 GHz and 3.5 GHz, and the beam directions are $\theta_{d1} = 90°$ and

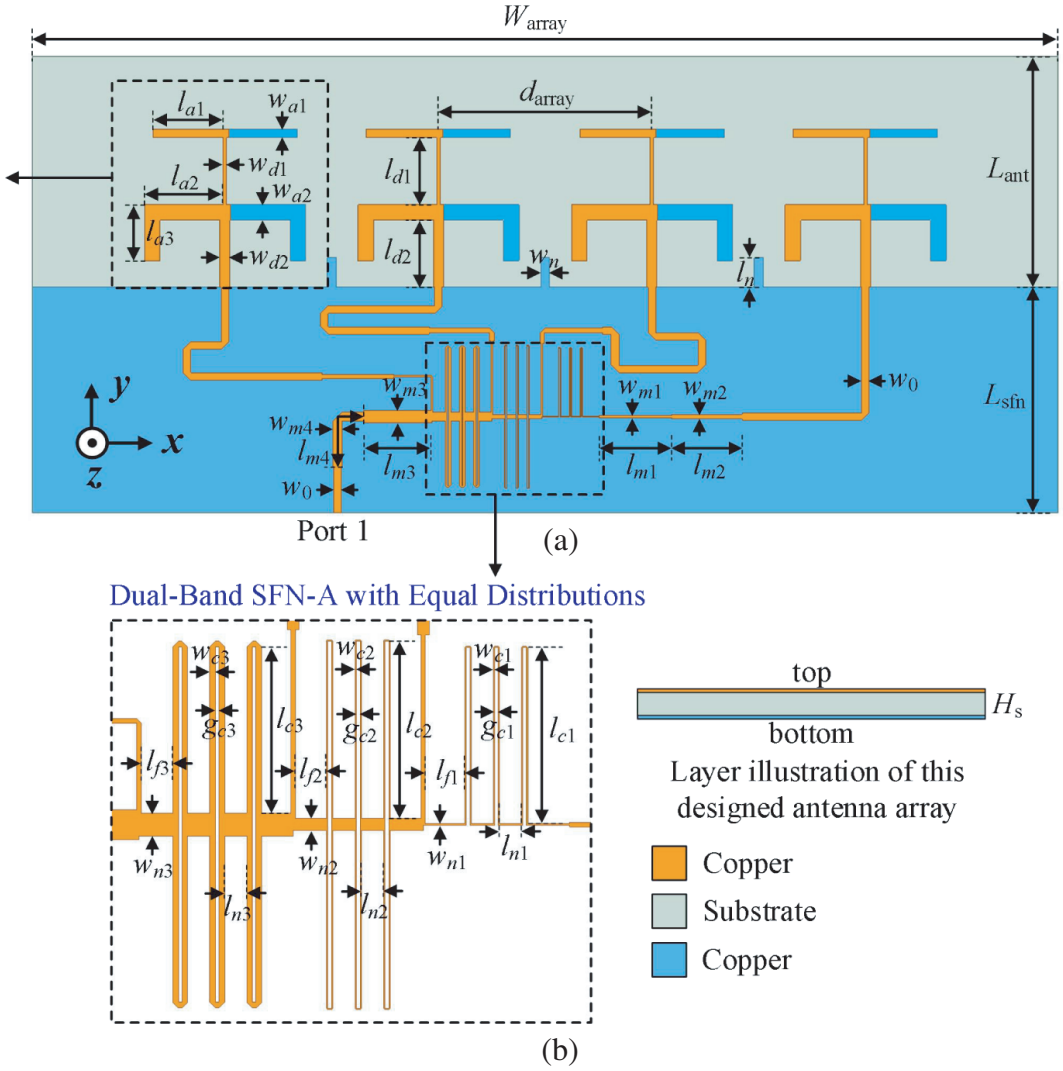

Figure 3. Structure of the designed dual-band SFA. (a) Total antenna array. (b) The proposed SFN.

$\theta_{d2} = 90°$ at two operating frequencies, respectively. The spacing between the antenna elements, d, is set to 50 mm, thus, the corresponding electrical length is $0.35\lambda_{low\_freq}$ and $0.58\lambda_{high\_freq}$. The structure of the designed SFA is drawn in Figure 3. The antenna is built on an RO4003C substrate with dielectric constant $\varepsilon_r = 3.55$, thickness $H_s = 0.813$ mm, and loss tangent $\tan\delta = 0.0027$.

For the dual-band SFA design, a dual-band antenna element with unidirectional radiation and wide beamwidth is required. As shown in the black dashed box in Figure 3(a), a dual-band antenna element is designed, which is developed from the work in [19] and [20]. The physical dimensions of the designed antenna element are tabulated in Table 1.

Table 1. Dimensions of the dual-band antenna element (Unit: mm).

l_{a1}	l_{a2}	l_{a3}	l_{d1}	l_{d2}	w_{a1}
16.4	18.4	13.3	16	16	2
w_{a2}	w_{d1}	w_{d2}	H_s		
3.6	0.83	2.3	0.813		

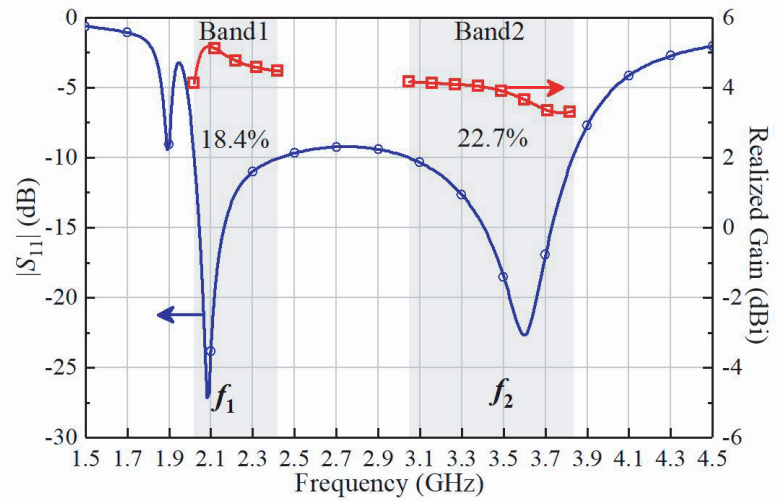

Figure 4. Simulated S_{11} and realized gain of the designed antenna element.

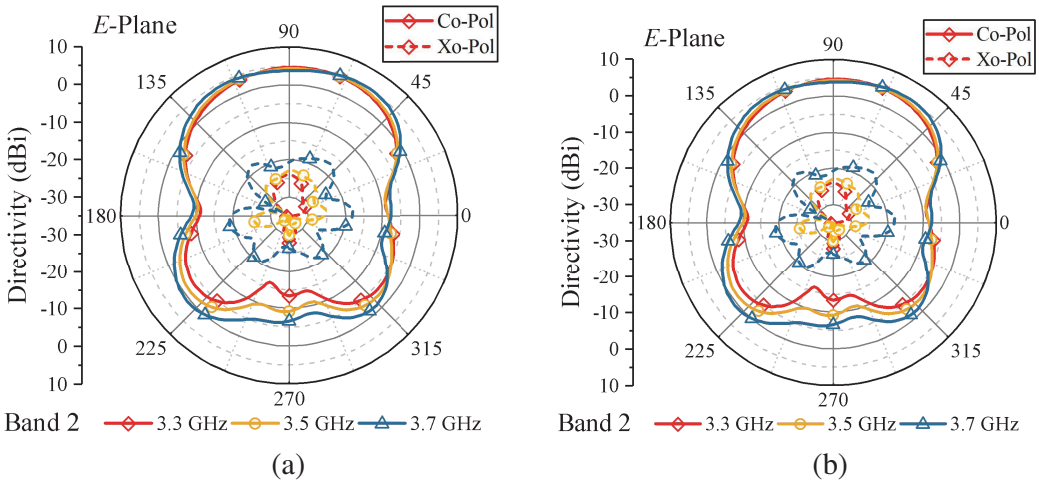

Figure 5. Simulated radiation patterns of designed dual-band antenna element in E-plane (xoy-plane in Figure 3). (a) Band 1. (b) Band 2.

Figure 4 illustrates the simulated S_{11} and realized gain in broadside direction for the designed dual-band antenna element. The simulated radiation patterns of this antenna element in two bands are shown in Figure 5 and Figure 6, respectively.

The optimized dimensions of the SFA are listed in Table 2. The simulated $|S_{11}|$ of dual-band SFA is shown in Figure 7. In terms of -10 dB impedance matching, the lower band ranges from 2.02 to 2.62 GHz (26.8%), and the higher band ranges from 2.87 to 4.02 GHz (33.4%).

The radiation patterns of designed dual-band SFA in the E-plane are shown in Figure 8. We can find that the steerable unidirectional radiation patterns are realized in the two bands. It is shown that the ranges of dual-band beam directions are from 70° to 95° and from 68° to 120°, respectively. The simulated maximum realized gain in the first frequency band (2.0–2.4 GHz) is 8.5 dBi, and in the second frequency band (3.1–3.8 GHz) is 9.2 dBi. For band 1, the broadside radiation ($\theta_{d1} = 90°$) is exactly achieved at the specified $f_1 = 2.1$ GHz. For band 2, the broadside radiation ($\theta_{d2} = 90°$) is achieved at $f_2 = 3.42$ GHz, which is slightly deviated from the specified 3.5 GHz.

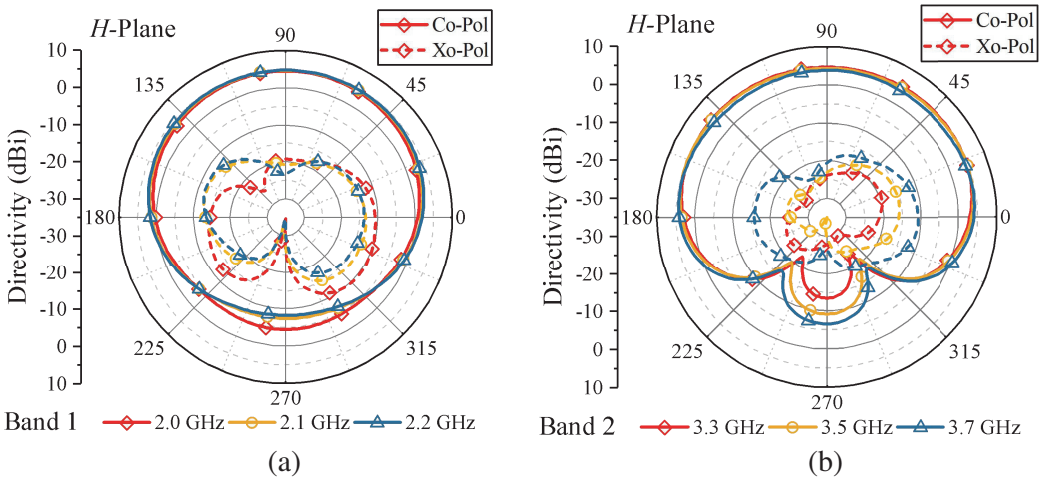

Figure 6. Simulated radiation patterns of designed dual-band antenna element in H-plane (yoz-plane in Figure 3). (a) Band 1. (b) Band 2.

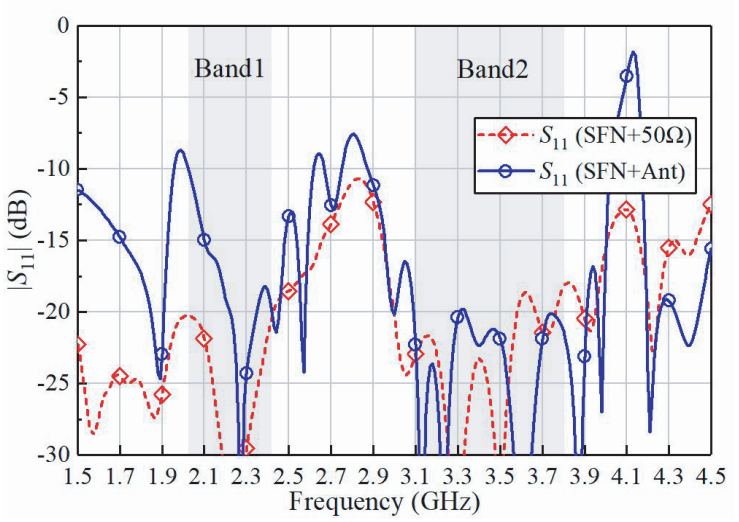

Figure 7. Simulated S_{11} of the proposed dual-band SFA.

Table 2. Dimensions of the proposed dual-band SFA (Unit: mm).

d_{array}	l_{c1}	l_{c2}	l_{c3}	l_{f1}	l_{f2}
50	16.3	16.4	15.4	3.6	2.8
l_{f3}	l_{m1}	l_{m2}	l_{m3}	l_{m4}	l_{n1}
2.9	17	16.6	15.8	15.8	2
l_{n2}	l_{n3}	w_{c1}	w_{c2}	w_{c3}	w_{m1}
2	2	0.1	0.1	0.52	0.4
w_{m2}	w_{m3}	w_{m4}	w_{n1}	w_{n2}	w_{n3}
1.05	2.8	2.2	0.15	1.1	2.1
g_{c1}	g_{c2}	g_{c3}	w_n	l_n	w_0
0.34	0.38	0.32	2	7	1.8

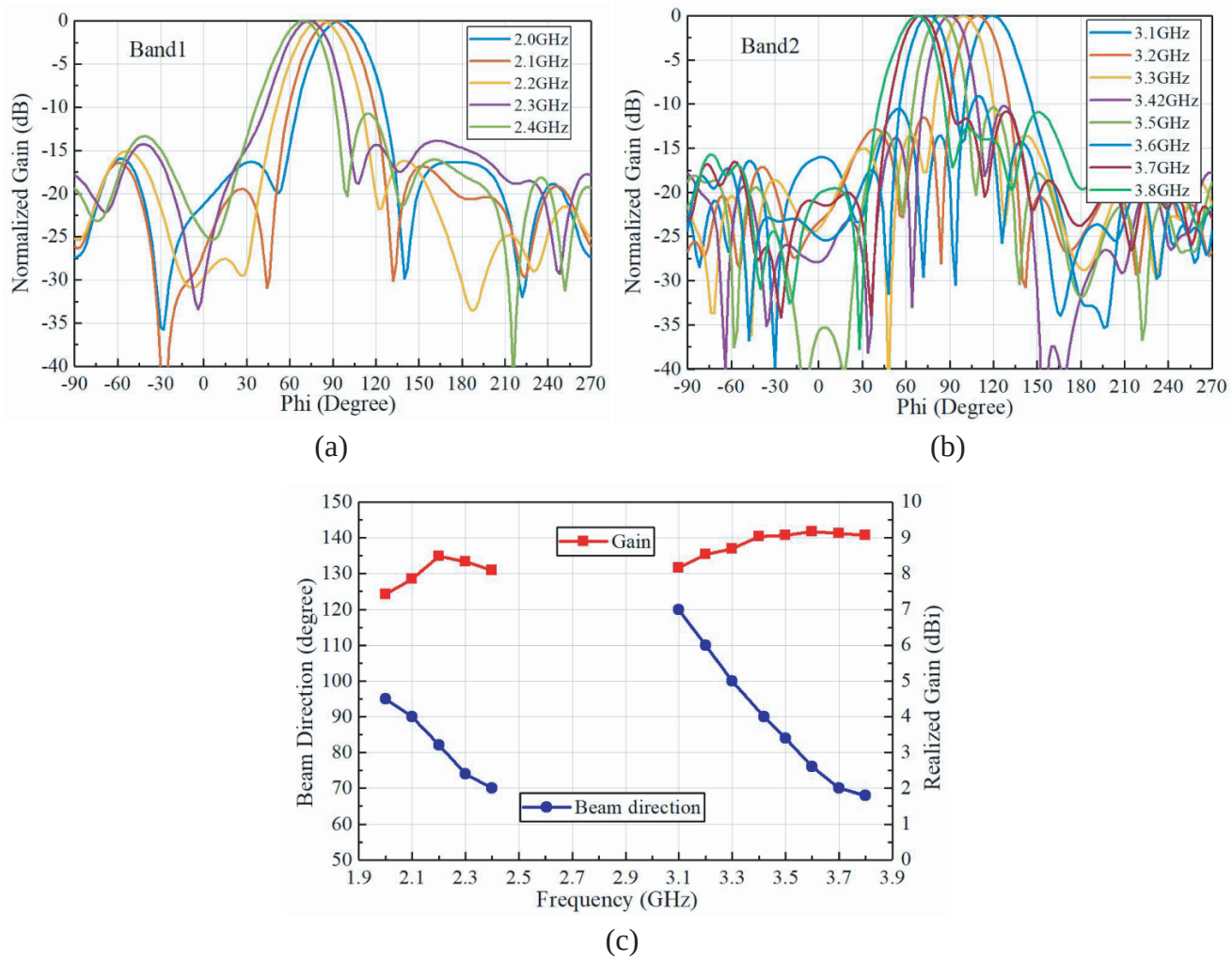

Figure 8. Simulated radiation pattern of the dual-band SFA in the *E*-plane. (a) Band 1. (b) Band 2. (c) Beam direction and realized gain.

3. MEASURED RESULTS

To verify the proposed SFA in Section 2, the antenna has been further fabricated and measured. Photographs of the fabricated antenna are shown in Figure 9. The reflection coefficient of the fabricated antenna is measured by the vector network analyzer Agilent E5071C and plotted in Figure 10. As shown in Figure 10, the $|S_{11}|$ is below -10 dB for both bands, which indicates good impedance matching of the proposed dual-band SFA.

The measurement of the radiation pattern and gain is carried out in a SATIMO near-field anechoic chamber as shown in Figure 11. The coordinate used by SATIMO Antenna Measurement System is also denoted in Figure 11.

The measured radiation patterns and gain are plotted in Figure 12 and Figure 13, respectively. The measured gain of lower band ranges from 7.0 dBi to 7.5 dBi, and the corresponding beam scans from -5 degrees to 25 degrees. For upper band, the measured gain ranges from 7.0 dBi to 8.5 dBi, and the corresponding beam scans from -20 degrees to 20 degrees. Meanwhile, the measured cross-polarization levels of the two bands are both below 18 dB, which indicates good linear polarization.

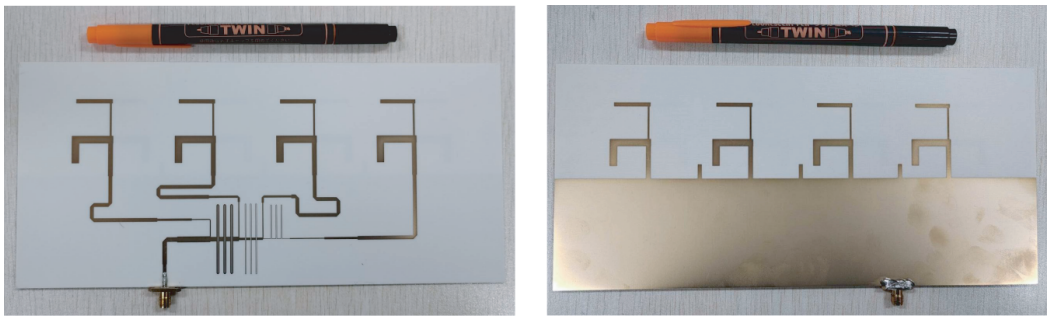

(a) (b)

Figure 9. The photograph of the fabricated antenna. (a) Front view; (b) Back view.

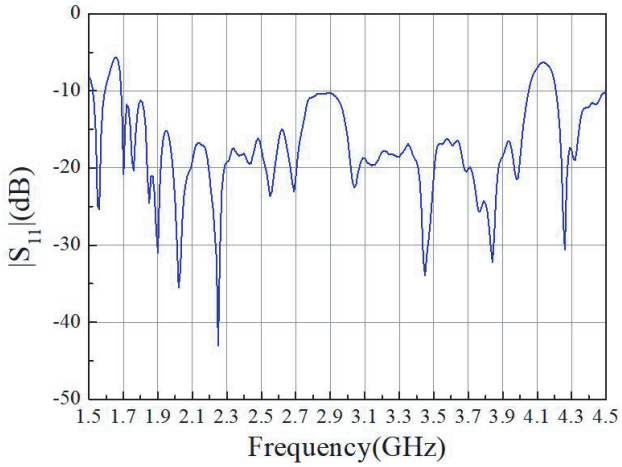

Figure 10. The measured reflection coefficient $|S_{11}|$.

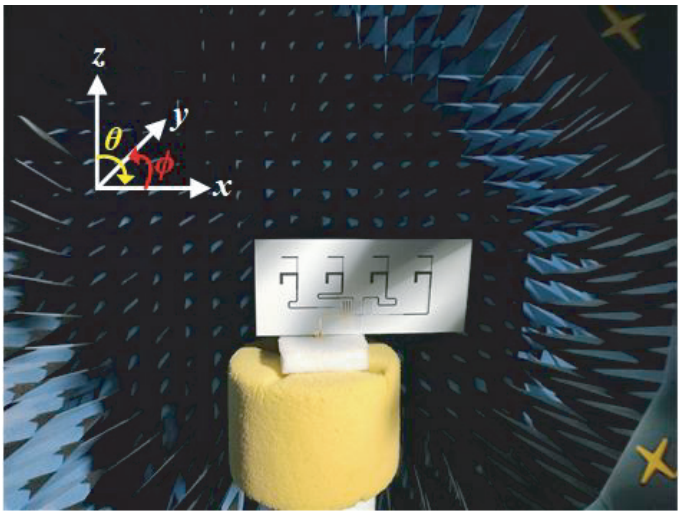

Figure 11. The photography of the fabricated SFA measured in the SATIMO near-filed anechoic chamber.

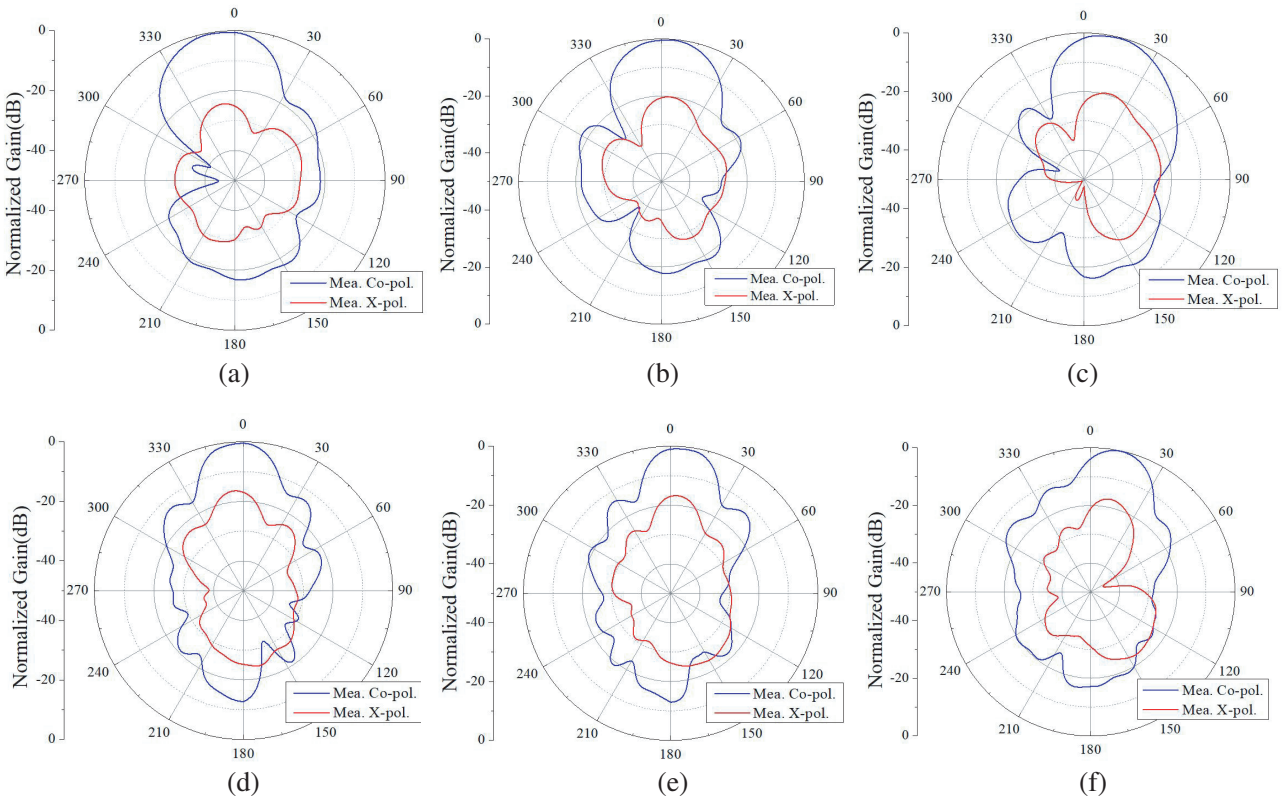

Figure 12. Measurement of the normalized radiation pattern of the dual-band SFA in the *xoz* plane. Band 1: (a) 2.0 GHz. (b) 2.1 GHz. (c) 2.2 GHz. Band 2: (d) 3.4 GHz. (e) 3.5 GHz. (f) 3.6 GHz.

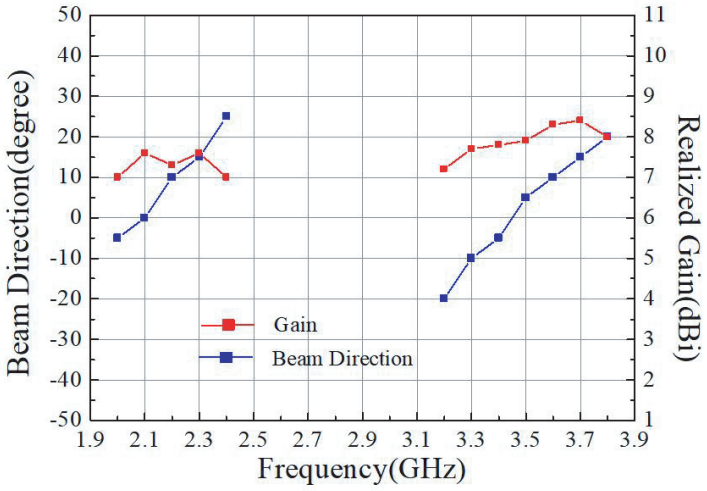

Figure 13. The measured gain of the dual-band SFA.

4. CONCLUSION

In this article, a novel dual-band SFA is presented. Based on the uniform TLs and C-sections, the beam directions of each band can be controlled independently. A design method for the proposed dual-band SFA is also presented. For verification, a prototype SFA with four elements is designed and measured. The measured results indicate that the proposed dual-band SFA features the advantage of independently controllable beam directions as predicted.

REFERENCES

1. Mailloux, R. J., *Phased Array Antenna Handbook*, 3rd Edition, Artech House, Norwood, MA, USA, 2017.
2. Wang, Z., G. Zhang, Y. Yin, and J. Wu, "Design of a dual-band high gain antenna array for WLAN and WiMAX base station," *IEEE Antennas Wireless Propag. Lett.*, Vol. 13, 1721–1724, 2014.
3. Yeung, S. H., A. García-Lampérez, T. K. Sarkar, and M. Salazar-Palma, "Thin and compact dual-band four-element broadside patch antenna arrays," *IEEE Antennas Wireless Propag. Lett.*, Vol. 13, 567–570, 2014.
4. Toh, W.-K., X.-M. Qing, and Z.-N. Chen, "A planar dual-band antenna array," *IEEE Trans. Antennas Propag.*, Vol. 59, No. 3, 833–838, Mar. 2011.
5. Zhang, X. Y., D. Xue, L. H. Ye, Y. M. Pan, and Y. Zhang, "Compact dual-band dual-polarized interleaved two-beam array with stable radiation pattern based on filtering elements," *IEEE Trans. Antennas Propag.*, Vol. 65, No. 9, 4566–4575, Sep. 2017.
6. Wei, D., J. Li, G. Yang, J. Liu, and J. Yang, "Design of compact dual-band SIW slotted array antenna," *IEEE Antennas Wireless Propag. Lett.*, Vol. 17, No. 6, 1085–1089, Jun. 2018.
7. Vetharatnam, G., C. B. Kuan, and C. H. Teik, "Combined feed network for a shared-aperture dual-band dual-polarized array," *IEEE Antennas Wireless Propag. Lett.*, Vol. 4, 297–299, 2005.
8. Wincza, K. and S. Gruszczynski, "Series-fed dual-band dual-polarized antenna lattice fed by slot-coupled power dividers," *IEEE Antennas Wireless Propag. Lett.*, Vol. 15, 1065–1068, 2016.
9. Jackson, D. R., C. Caloz, and T. Itoh, "Leaky-wave antennas," *Proc. IEEE*, Vol. 100, No. 7, 2194–2206, Jul. 2012.
10. Machac, J., M. Polivka, and K. Zemlyakov, "A dual band leaky wave antenna on a CRLH substrate integrated waveguide," *IEEE Trans. Antennas Propag.*, Vol. 61, No. 7, 3876–3879, Jul. 2013.
11. Simorangkir, R. B. V. B. and Y. Lee, "A planar dual-band periodic leakywave antenna based on a mu-negative (MNG) transmission line," *IEEE Trans. Antennas Propag.*, Vol. 63, No. 5, 2370–2374, May 2015.
12. Karmokar, D. K. and K. P. Esselle, "Periodic U-slot-loaded dual-band halfwidth microstrip leaky-wave antennas for forward and backward beam scanning," *IEEE Trans. Antennas Propag.*, Vol. 63, No. 12, 5372–5381, Dec. 2015.
13. Li, Y. and J. Wang, "Dual-band leaky-wave antenna based on dual-mode composite microstrip line for microwave and millimeter-wave applications," *IEEE Trans. Antennas Propag.*, Vol. 66, No. 4, 1660–1668, Apr. 2018.
14. Otto, S., A. Rennings, O. Litschke, and K. Solbach, "A dual-frequency series-fed patch array antenna," *Proc. IEEE EuCAP*, 1171–1175, 2009.
15. Chioukh, L., H. Boutayeb, D. Deslandes, and K. Wu, "Dual-band linear antenna array for harmonic sensing applications," *IEEE Antennas Wireless Propag. Lett.*, Vol. 15, 1577–1580, 2016.
16. Zhang, Y., X.-Y. Zhang, and Y.-M. Pan, "Compact single-and dual-band filtering patch antenna arrays using novel feeding scheme," *IEEE Trans. Antennas Propag.*, Vol. 65, No. 8, 4057–4066, Aug. 2017.
17. Schiffman, B. M., "A new class of broad-band microwave 90-degree phase shifters," *IRE Trans. Microw. Theory Techn.*, Vol. 6, No. 2, 232–237, Apr. 1958.
18. Lyu, Y.-P., L. Zhu, and C.-H. Cheng, "Design and analysis of Schiffman phase shifter under operation of its second phase period," *IEEE Trans. Microw. Theory Techn.*, Vol. 66, No. 7, 3263–3269, Jul. 2018.
19. Tefiku, F. and C. A. Grimes, "Design of broad-band and dual-band antennas comprised of series-fed printed-strip dipole pairs," *IEEE Trans. Antennas Propag.*, Vol. 48, 895–900, Jun. 2000.
20. Huang, H., J. Lu, and P. Hsu, "A compact dual-band printed Yagi-Uda antenna for GNSS and CMMB applications," *IEEE Trans. Antennas Propag.*, Vol. 63, No. 5, 2342–2348, May 2015.